Violet to deep-ultraviolet InGaN/GaN and GaN/AlGaN quantum structures for UV electroabsorption modulators

Tuncay Ozel, Emre Sari, Sedat Nizamoglu, and Hilmi Volkan Demir[a)]
Department of Physics, Department of Electrical and Electronics Engineering, and Nanotechnology Research Center, Bilkent University, Ankara TR-06800, Turkey

(Received 2 August 2007; accepted 3 October 2007; published online 3 December 2007)

In this paper, we present four GaN based polar quantum structures grown on *c*-plane embedded in *p-i-n* diode architecture as a part of high-speed electroabsorption modulators for use in optical communication (free-space non-line-of-sight optical links) in the ultraviolet (UV): the first modulator incorporates ~4–6 nm thick GaN/AlGaN quantum structures for operation in the deep-UV spectral region and the other three incorporate ~2–3 nm thick InGaN/GaN quantum structures tuned for operation in violet to near-UV spectral region. Here, we report on the design, epitaxial growth, fabrication, and characterization of these quantum electroabsorption modulators. In reverse bias, these devices exhibit a strong electroabsorption (optical absorption coefficient change in the range of 5500–13 000 cm^{-1} with electric field swings of 40–75 $V/\mu m$) at their specific operating wavelengths. In this work, we show that these quantum electroabsorption structures hold great promise for future applications in ultraviolet optoelectronics technology such as external modulation and data coding in secure non-line-of-sight communication systems. © *2007 American Institute of Physics*. [DOI: 10.1063/1.2817954]

INTRODUCTION

To date, significant progress has been achieved in GaN based optoelectronics industry.[1,2] In the visible spectral range, light emitting diodes,[3] laser diodes,[4] and electroabsorption modulators[5] have been demonstrated. Nowadays, a special interest of scientific research is also focused on the demonstration of ultraviolet (UV) optoelectronic devices. Such devices hold promise for applications especially in non-line-of-sight (NLOS) communication systems. A chip-scale UV light source is considered as one of the strongest candidates for use in such NLOS communication.[6] However, for future high-speed NLOS communication, the introduction of external modulation is necessary if higher bit rate data links are desired to be achieved. Today, although rf wireless communication technology is well developed and commonly used,[7] it fails in fulfilling the security aspects of the communication. In NLOS UV communication, the atmospheric and particle scattering effectively entangles unwanted incoming links, making this type of communication systems absolutely secure.[8,9] This promising application field necessitates the demonstration of high-speed quantum electroabsorption modulators that incorporate GaN based quantum structures for use in high bit rate data links in UV. For NLOS communication systems, such a quantum electroabsorption modulator is a chip-scale solution, providing the important advantages of portability and low power consumption as required by specific applications (for example, in autonomous vehicles). However, material related problems complicate the growth of such optoelectronic devices operating at short wavelengths. With the use of InGaN/GaN quantum structures, optoelectronic devices operating in visible to near UV are feasible, whereas deep-UV optoelectronic devices require the use of GaN/AlGaN quantum structures.[10–12] AlGaN based quantum structures, however, exhibit technical difficulties such as relatively slow growth rates, high dislocation densities of Al, and insufficient conductivity of doped layers.[13] In this work, to this end, we demonstrate four different quantum electroabsorption modulators with their operating wavelengths spanning from 400 to 270 nm by using InGaN and AlGaN based quantum structures in their active region as required for operating in visible to near-UV and deep-UV spectral ranges, respectively. Based on our proof-of-concept demonstrations here, such UV electroabsorption quantum structures hold great promise for use in future high-speed NLOS communication applications.

In this paper, we present the design, epitaxial growth, fabrication, and characterization of such quantum electroabsorption modulators operating in their specific wavelength ranges (<400 nm). The electroabsorption properties of GaN/AlGaN quantum structures in the UV (~350 nm) were previously characterized successfully in the work of Friel *et al.*[14] Here, for the first time, we report on the electroabsorption characterization of polar InGaN/GaN quantum structures in the violet (~400 nm) and polar GaN/AlGaN quantum structures in the deep UV (<300 nm), all grown on sapphire.

EXPERIMENTAL

For the growth of our epitaxial layer designs, we use a GaN dedicated Aixtron RF-200 metal organic chemical vapor deposition system located at Bilkent University Nanotechnology Research Center. We use double side-polished *c*-plane sapphire as the substrate and TE-Ga (for Ga in quantum structures), TM-Ga (for Ga in bulk layers), TM-Al, TM-

[a)]Tel.: [+90](312) 290-1021. FAX: [+90](312) 290-1015. Electronic mail: volkan@bilkent.edu.tr

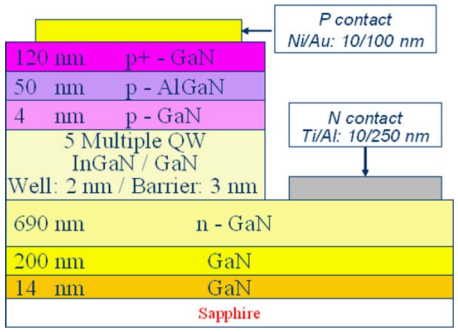

FIG. 1. Illustration of the epitaxial layer design of our InGaN/GaN based quantum electroabsorption modulator (QEM-3 and QEM-4) along with the fabricated contacts.

In, and NH_3 as the precursors. Our quantum electroabsorption modulator designs are based on *p-i-n* diode architectures with the intrinsic region incorporating unintentionally doped InGaN/GaN or GaN/AlGaN quantum structures. For GaN/AlGaN based quantum electroabsorption modulator (QEM-1), we start the epitaxial growth with 15 nm thick low temperature AlN nucleation and 150 nm thick high temperature AlN buffer layers. Following an undoped 150 nm AlGaN layer, we grow 150 nm Si doped *n*-type AlGaN layer. The active region houses an unintentionally doped AlGaN multiple quantum well structure (four sets of 4 nm thick well and 6 nm thick barrier.) Active region is capped with a 40 nm thick *p*-type AlGaN layer. Finally, a very thin 10 nm highly Mg doped *p*-type contact layer is grown. For the InGaN/GaN based quantum electroabsorption modulators (QEM-2, -3, and -4), we start the epitaxial growth with 14 nm thick GaN nucleation layer and 200 nm thick GaN buffer layer; QEM-3 structure is shown in Fig. 1. A 690 nm thick Si doped *n*-type GaN layer is subsequently grown. The active regions embody multiple quantum wells and barriers, each with ~2–3 nm thick grown consecutively. Different growth temperatures are used for the active region to modify the operation wavelength of our modulators. For QEM-2, QEM-3, and QEM-4, the growth temperatures of 705, 710, and 720 °C are used, respectively, which tunes the amount of In incorporation and thus the absorption band edge (i.e., the operating wavelength), as also studied in our previous work.[15,16] The epitaxial growth is monitored at all times by *in situ* optical reflectance, and the growth temperature is further controlled using two infrared pyrometers. For QEM-2,

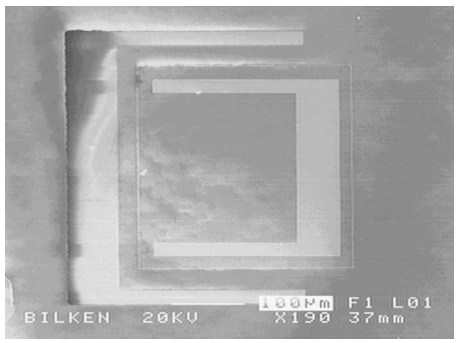

FIG. 2. Scanning electron microscope image of one of our fabricated quantum electroabsorption modulators.

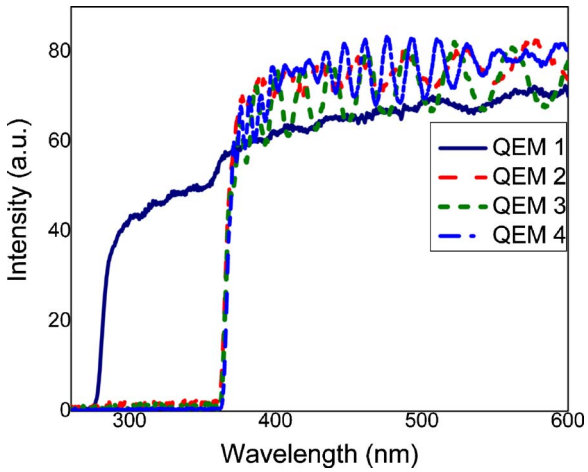

FIG. 3. Optical transmission spectrum of our epitaxially grown quantum electroabsorption modulators.

we only grow 4 nm thick Mg doped *p*-type contact layer. For QEM-3 and QEM-4, following the active region, we grow 50 nm thick *p*-type AlGaN layer and finally 120 nm thick Mg doped *p*-type GaN layer on the top. For the activation of Mg dopants, we anneal the wafers at 750 °C for 15 min.

We use standard semiconductor fabrication processes[17] including photolithography, reactive ion etching (RIE), metal deposition, and rapid thermal annealing using class-100 cleanroom facilities of Bilkent University Advanced Research Laboratories and Nanotechnology Research Center, as also described in our previous work.[18–20] We use RIE to etch down to the middle of *n* layer to define device mesas, as illustrated in Fig. 1. We lay down Ni/Au (10/100 nm) and Ti/Al (10/250 nm) for *p* and *n* contacts, respectively. We perform *p*-contact rapid thermal annealing to form the Ohmic contact at 700 °C for 30 s for InGaN based QEMs and 825 °C for 60 s for AlGaN based QEM. The contacts are finally annealed at 600 °C for 1 min under N_2 purge. The fabricated devices have mesa sizes varying from 10 $\times$ 10 to 300 $\times$ 300 μm^2 and also feature open optical windows to couple light into the device from the top and to collect the output light from the transparent substrate on the

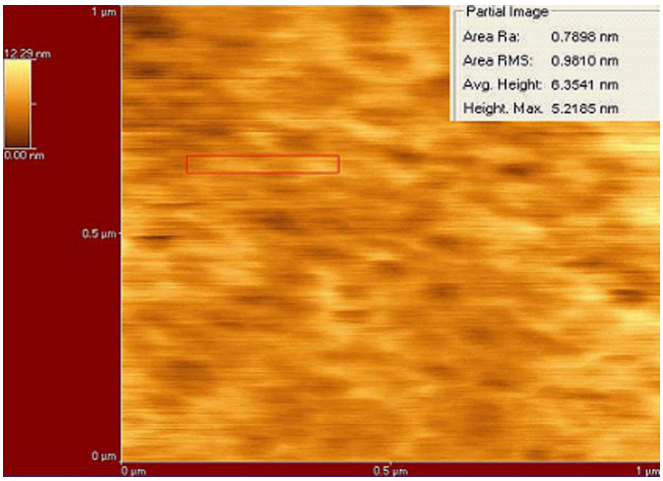

FIG. 4. Atomic force microscope image of one of our quantum electroabsorption modulators.

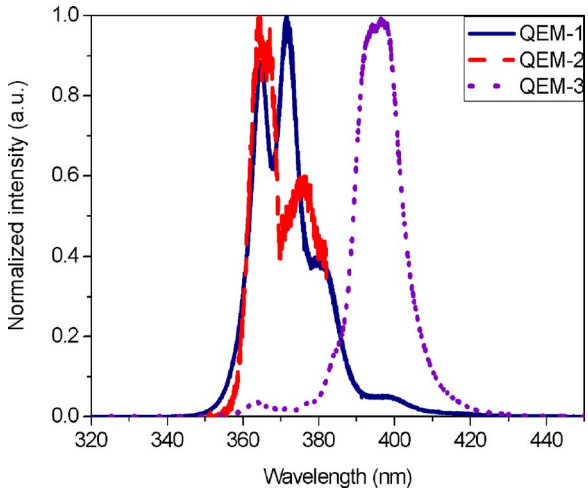

FIG. 5. Normalized photoluminescence spectra of our InGaN/GaN based QEM-2 and QEM-3 at room temperature.

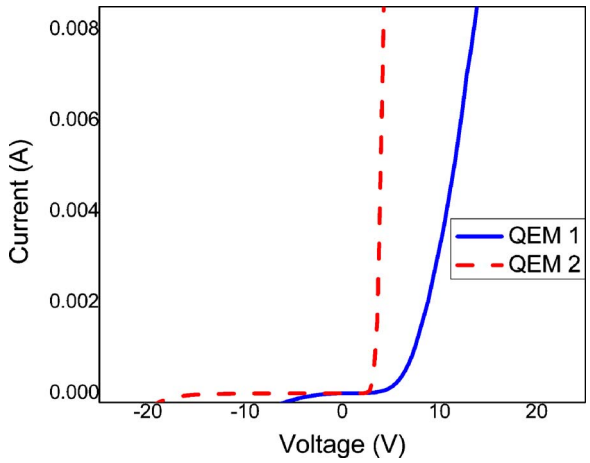

FIG. 6. Current-voltage characteristics of the fabricated devices with a top-view micrograph of one of our fabricated quantum electroabsorption modulators.

bottom during operation. Figure 2 depicts the scanning electron microscope image of our fabricated device, which shows the device mesa with its *p* contact on the top and its *n* contact on the bottom.

RESULTS AND DISCUSSIONS

We perform the characterization in two steps: first, surface and optical characterizations on the unprocessed wafer, and second, electrical characterization on the processed devices. We obtain optical transmission spectra of the epitaxially grown wafers with the use of a UV-visible xenon lamp and a spectrometer. As depicted in Fig. 3, the optical transmission spectra of our AlGaN based design have absorption band edge around 265 nm and InGaN based designs around 360 nm, which also confirms that our epitaxial structures are designed with the right band edge for operation in the expected UV spectral range.

We use an atomic force microscope (AFM) for surface characterization of the QEM wafers to detect if any growth related cracks exist. In Fig. 4, we observe that the root-mean-square roughness of our epitaxially grown structures is less than 1 nm. The roughness level of the wafer surface confirms that our epitaxial growth is successfully controlled. In AFM characterization, no cracking is observed.

We perform photoluminescence (PL) characterization by using a high power He–Cd laser with an excitation wavelength of 325 nm at room temperature. In Fig. 5, we observe the PL peaks of InGaN housing QEM-2 and QEM-3 structures. For QEM-2, we observe the PL peak at 371 nm with a full width at half maximum (FWHM) of 10 nm, for QEM-3, PL peak at 376 nm with a FWHM of 12 nm, and for QEM-4, PL peak at 396 nm with a FWHM of 14 nm. These PL spectra confirm that our epitaxial designs feature the proper concentration of $In_xGa_{(1-x)}N/GaN$ quantum structures as targeted (with $x=0.02$ for QEM-2, $x=0.04$ for QEM-3, and $x=0.12$).

Following the optical characterization, we perform electrical characterization on the fabricated devices. We use HP 4142 parameter analyzer for the current-voltage (*I-V*) characterization of the diode. As shown in Fig. 6, the general diode performance for InGaN based QEMs features a turn-on voltage at 3 V and the in-series parasitic resistance is mea-

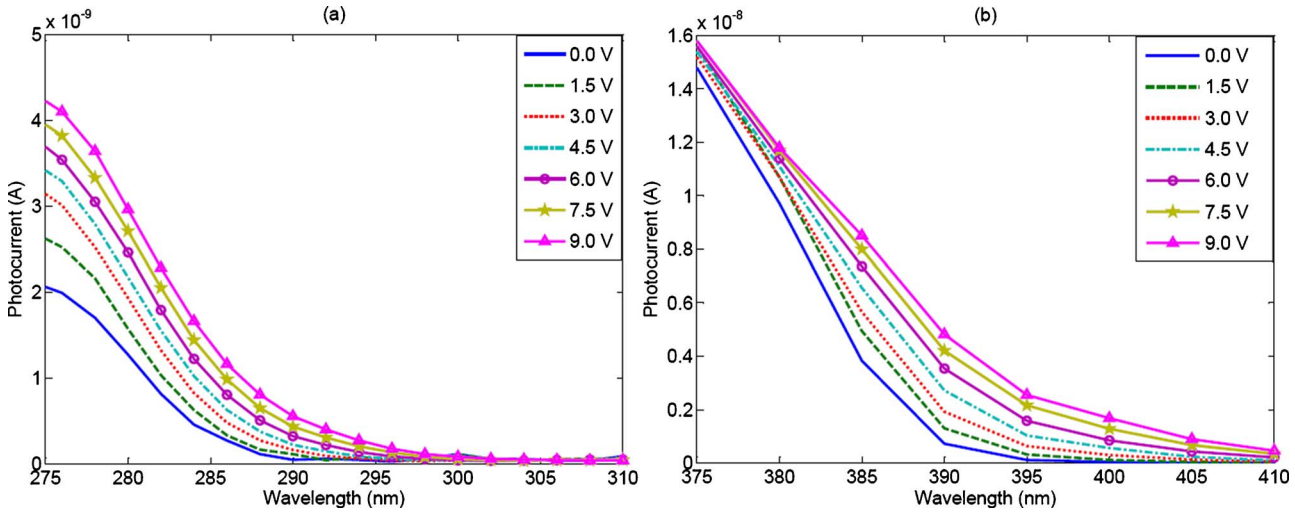

FIG. 7. Photocurrent spectra of (a) AlGaN based QEM-1 and (b) InGaN based QEM-3 at room temperature.

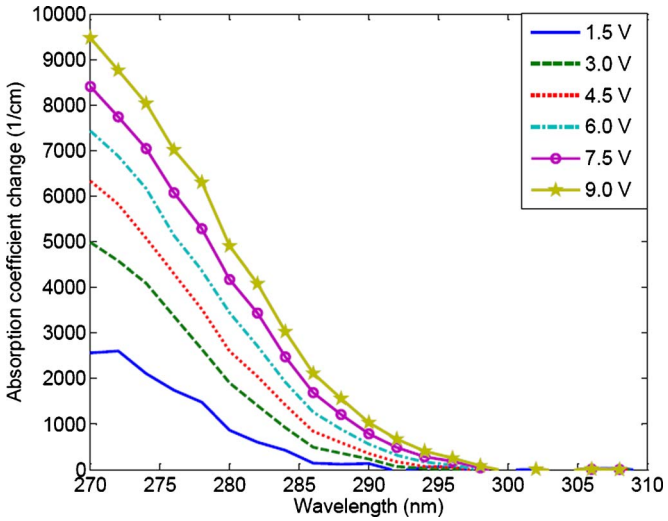

FIG. 8. Absorption coefficient change spectrum of AlGaN based deep-UV QEM-1.

sured to be ~80 Ω. Such low in-series parasitic resistance overcomes the local heating problem of the diode. On the other hand, AlGaN based diode features a turn on at 6 V and its in-series parasitic resistance is measured to be ~600 Ω. This considerably high resistance is due to the insufficient conductivity of *p*-type AlGaN layer.[13] This resistance level is one of the issues that reduce the performance of the QEM-1 structure. Given their mesa size of 10×10 μm^2, their corresponding device capacitance is ~0.15–0.3 pF, corresponding to *RC* time constants of ~90 ps for QEM-1 and ~25 ps for QEM-2, -3, and -4, respectively. In principle, this would safely enable these devices to operate in the gigahertz range.

We perform photocurrent measurements with an optical setup that consists of a xenon light source, a monochromator, a chopper, and a lock-in amplifier by applying reverse biases across the devices. Figures 7(a) and 7(b) show the photocurrent spectrum of QEM-1 and QEM-3 parametrized at reverse biases from 0 to 9 V swing (in 1.5 V steps), respectively. In this measurement, the level of dark current is in the range of a few nanoamperes. Here, we encounter carrier collection problem in the AlGaN based QEM-1. This carrier collection problem is one of the major issues that undesirably affect the device operation.[21]

We calculate the electroabsorption spectra by using the photocurrent data at various levels of the applied voltages. We process the electroabsorption data and convert into the absorption coefficient spectrum. We simply measure the quantum efficiencies of the devices by using the spectral responsivity curve. We take the Fresnel reflection into account and assume that all generated electron-hole pairs due to the optical absorption process contribute to the photocurrent.[12,13] Here, we take the thickness of the total absorption layer as the thickness of whole active region including all the quantum wells and barriers. [In the previous characterization of a UV modulator by Friel *et al.*, the thickness of the absorbing layer is considered to consist of only the thickness of only quantum wells.[14] However, it should be noted that the incoming light is also absorbed by the barriers (as these are typically coupled quantum structures and the wavefunctions penetrate well into the barriers)]. Figure 8 shows the optical absorption coefficient change of QEM-1 incorporating AlGaN at each applied bias level with respect to the 0 V curve. As depicted in Fig. 8, AlGaN based QEM-1 exhibits a 9500 cm^{-1} absorption coefficient change at 275 nm with an applied reverse bias of 9 V (corresponding to an electric field swing of 50 V/μm) in the spectral range where it is transmissive, as also shown in the transmission spectrum in Fig. 3. This GaN/AlGaN based quantum electroabsorption modulator operating at 270 nm features a sufficiently high absorption coefficient change, which is comparable to the previous work of Friel *et al.* for operation at ~355 nm.[14] (Here, note that if only wells were taken as the thickness of the absorbing layer, this absorption coefficient change would be calculated to be 2.4×10^4 cm^{-1}.) For the InGaN based QEMs, we observe that QEM-2 exhibits an absorption coefficient change of 13 000 cm^{-1} at 380 nm, QEM-3 exhibits an absorption coefficient change of 6500 cm^{-1} at 385 nm, and QEM-4 exhibits an absorption coefficient change of 5500 cm^{-1} at 400 nm with an applied reverse bias of 9 V (corresponding to electric field swings of 75, 50, and 40 V/μm, respectively), as shown in Fig. 9. This achieved electromodulation is the highest in InGaN/GaN based quantum structures compared to the previous reports.[5,22,23] (Also, here note that if only wells were taken as the thickness of the absorbing layer, these absorption coefficient changes would then be calculated to be even further larger with the respective values of 3.1×10^4, 1.5×10^4, and 1.3×10^4 cm^{-1}.) The absorption coefficient changes of these GaN/AlGaN based and InGaN/GaN based quantum electroabsorption modulators implies that an ~50 μm long waveguide modulator with

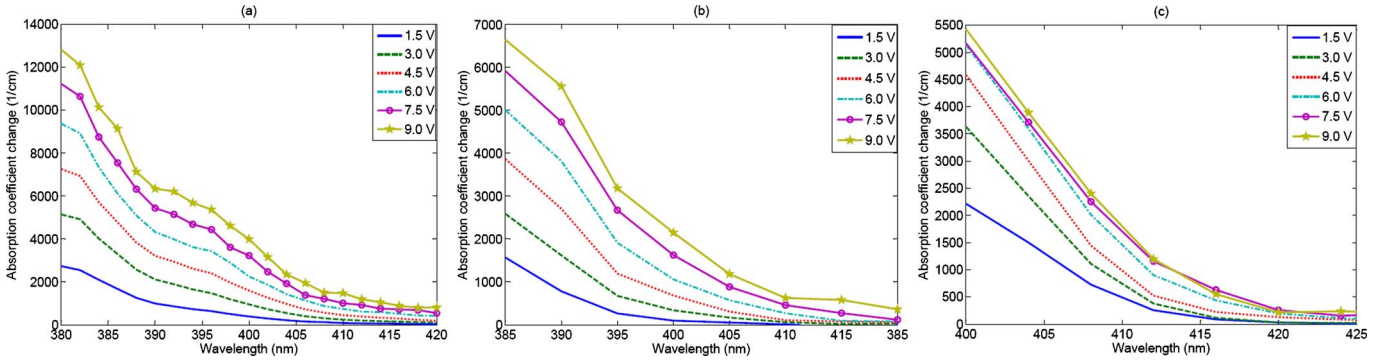

FIG. 9. Absorption coefficient change spectra of InGaN based (a) near-UV QEM-2, (b) near-UV QEM-3, and (c) violet QEM-4.

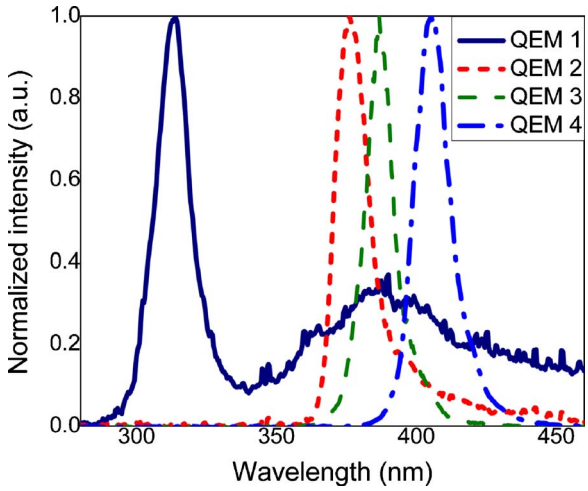

FIG. 10. Normalized electroluminescence spectrum of all quantum electroabsorption modulators (QEM-1, −2, −3, and −4).

a reasonable overlap integral of the waveguide mode with the quantum structures (e.g., $\Gamma \sim 0.1$) is expected to achieve a 10 dB contrast ratio for a 2 V/μm field swing.

Moreover, in forward bias operation, QEM-1 features an electroluminescence (EL) peak at 313 nm with a FWHM of 14 nm, as shown in Fig. 10. However, there is a wide and unexpected emission around 380 nm, which is possibly caused by the impurities introduced during the epitaxial growth. QEM-2 features an EL peak at 375 nm with a FWHM of 13 nm, QEM-3 features an EL peak at 386 nm with a FWHM of 12 nm, and QEM-4 features an EL peak at 405 nm with a FWHM of 15 nm. For QEM-2 and QEM-3, EL peaks are sharp and in good agreement with the PL spectrum shown in Fig. 5. As expected, compared to the PL peaks in Fig. 5, we observe a redshift in EL peaks of QEMs in Fig. 10. The output power collected from one side of the QEM-1 is in the submicrowatt range and from QEM-2, -3, and -4, it is in the submilliwatt range.

CONCLUSIONS

In this work, we developed and demonstrated four quantum electroabsorption modulators: one AlGaN based modulator operating in the deep UV (270 nm), two InGaN based modulator operating at near UV (375 and 385 nm), and one InGaN based modulator operating in the violet (400 nm) spectral region with high absorption coefficient changes from 5500 up to 13 000 cm^{-1} for an applied reverse bias change of 9 V (corresponding to 40–75 V/μm electric field swing). These quantum electroabsorption modulators also emit light as a second mode of operation when forward bias is applied across the devices. Here, for the first time, we demonstrated and characterized InGaN based violet quantum electroabsorption modulators and AlGaN based deep-UV quantum electroabsorption modulators. With this work, we realized strong electroabsorption using AlGaN based modulators in the UV range, suggesting that there is a high potential for their use in future non-line-of-sight communication applications.

ACKNOWLEDGMENTS

This work is supported by EU-PHOREMOST Network of Excellence 511616 and Marie Curie European Reintegration Grant No. MOON 021391 within the 6th European Community Framework Program and TUBITAK under the Project Nos. EEEAG 104E114, 106E020, 105E065, and 105E066. The authors acknowledge additional support from the Turkish National Academy of Sciences Distinguished Young Scientist Award (TÜBA GEBİP), European Young Investigator (EURYI) Award, and TUBITAK Fellowship Programs. The authors also thank Yilmaz Dikme, Serkan Butun, and Nihan Kosku Perkgoz for their fruitful discussions and useful contributions. The authors are pleased to acknowledge the Bilkent University Nanotechnology Research Center and Advanced Research Laboratories for allowing them to use their facilities for this work.

[1] S. P. Denbaars, Proc. IEEE **85**, 1740 (1997).
[2] M. A. Khan, M. Shatalov, H. P. Maruska, H. M. Wang, and E. Kuokstis, Jpn. J. Appl. Phys., Part 1 **44**, 7191 (2005).
[3] E. Fred Schubert, *Light Emitting Diodes* (Cambridge University Press, New York, 2006).
[4] S. Nakamura, G. Fasol, and S. J. Pearton, *The Blue Laser Diode: The Complete Story* (Springer, New York, 2000).
[5] E. Sari, S. Nizamoglu, T. Ozel, and H. V. Demir, Appl. Phys. Lett. **90**, 011101 (2007).
[6] A. M. Siegel, G. A. Shaw, and J. Model, Proc. SPIE **5417**, 214 (2004).
[7] T. S. Rappaport, *Wireless Communications: Principles and Practice* (IEEE, Piscataway, NJ, 1996).
[8] G. A. Shaw, A. M. Siegel, and J. Model, IEEE LEOS Newsletter **19**, 5 (2005).
[9] D. E. Sunstein, "A Scatter Communications Link at Ultraviolet Frequencies," Thesis, MIT, 1968.
[10] S. F. Chichibu, A. Shikanai, T. Deguchi, A. Setoguchi, R. Nakai, H. Nakanishi, K. Wada, S. P. DenBaars, T. Sota, and S. Nakamura, Jpn. J. Appl. Phys., Part 1 **39**, 2417 (2000).
[11] D. M. Graham, A. Soltani-Vala, P. Dawson, M. J. Godfrey, T. M. Smeeton, J. S. Barnard, M. J. Kappers, C. J. Humphreys, and E. J. Thrush, J. Appl. Phys. **97**, 103508 (2005).
[12] A. A. Allerman, M. H. Crawford, A. J. Fischer, K. H. A. Bogart, S. R. Lee, D. M. Follstaedt, P. P. Provencio, and D. D. Koleske, J. Cryst. Growth **272**, 227 (2004).
[13] I. Akasaki and H. Amano, Jpn. J. Appl. Phys., Part 1 **36**, 5393 (1997).
[14] I. Friel, C. Thomidis, and T. D. Moustakas, J. Appl. Phys. **97**, 123515 (2005).
[15] S. Nizamoglu, T. Ozel, E. Sari, and H. V. Demir, Nanotechnology **18**, 065709 (2007).
[16] H. V. Demir, S. Nizamoglu, T. Ozel, E. Mutlugun, I. O. Huyal, E. Sari, E. Holder, and N. Tian, New J. Phys. **9**, 362 (2007).
[17] P. Schlotter, J. Baur, Ch. Hielscher, M. Kunzer, H. Obloh, R. Schmidt, and J. Schneider, Mater. Sci. Eng., B **59**, 390 (1999).
[18] H. V. Demir, V. A. Sabnis, O. Fidaner, J. S. Harris, D. A. M. Miller, and J. F. Zheng, IEEE J. Sel. Top. Quantum Electron. **11**, 86 (2005).
[19] H. V. Demir, V. A. Sabnis, J. F. Zheng, O. Fidaner, J. S. Harris, and D. A. B. Miller, IEEE Photonics Technol. Lett. **16**, 2305 (2004).
[20] V. A. Sabnis, H. V. Demir, O. Fidaner, J. S. Harris, D. A. B. Miller, J. F. Zheng, N. Li, T. C. Wu, H. T. Chen, and Y. M. Houng, Appl. Phys. Lett. **84**, 469 (2004).
[21] H. Shichijo, R. M. Kolbas, N. Holonyak, R. D. Dupuis, and P. D. Dapkus, Solid State Commun. **27**, 10 (1978).
[22] A. E. Oberhofer, J. F. Muth, M. A. L. Johnson, Z. Y. Chen, E. F. Fleet, and G. D. Cooper, Appl. Phys. Lett. **83**, 2748 (2003).
[23] M. Kneissl, T. L. Paoli, P. Kiesel, D. W. Treat, M. Teepe, N. Miyashita, and N. M. Johnson, Appl. Phys. Lett. **80**, 3283 (2002).